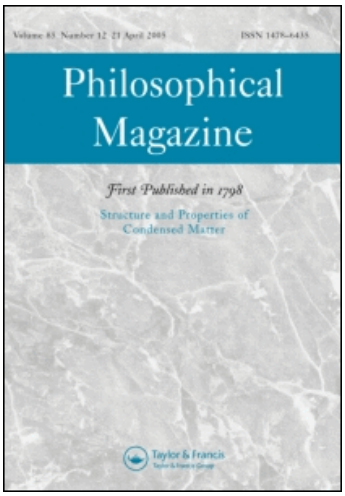

Philosophical Magazine
Publication details, including instructions for authors and subscription information:
http://www.informaworld.com/smpp/title~content=t713695589

Cross-sectional transmission electron microscopy of ultra-fine wires of AISI 316L stainless steel

H. S. Wang [a]; R. C. Wei [a]; C. Y. Huang [a]; J. R. Yang [a]
[a] Department of Materials Science and Engineering, National Taiwan University, Taipei, Taiwan, ROC

Online Publication Date: 11 January 2006

To cite this Article Wang, H. S., Wei, R. C., Huang, C. Y. and Yang, J. R.(2006)'Cross-sectional transmission electron microscopy of ultra-fine wires of AISI 316L stainless steel',Philosophical Magazine,86:2,237 — 251
To link to this Article: DOI: 10.1080/14786430500254271
URL: http://dx.doi.org/10.1080/14786430500254271

Philosophical Magazine,
Vol. 86, No. 2, 11 January 2006, 237–251

Taylor & Francis
Taylor & Francis Group

Cross-sectional transmission electron microscopy of ultra-fine wires of AISI 316L stainless steel

H. S. WANG*, R. C. WEI, C. Y. HUANG† and J. R. YANG

Department of Materials Science and Engineering,
National Taiwan University, Taipei, Taiwan, ROC

(*Received 18 April 2005; in final form 21 June 2005*)

Starting with 190 μm diameter wire of 316L stainless steel, ultra-thin wire just 8 μm in diameter has been made and characterized. There was no intermediate heat treatment used in the process of drawing, and the amount of true stain was about 6.3. A specimen preparation method for the cross-sectional transmission electron microscopy (TEM) of ultra-fine wires of 316L stainless steel has been developed. The ultra-fine wire was sandwiched between silicon chips and the bonded assembly then sliced to produce longitudinal and transverse sections of the wire in a form suitable for further processing into electron transparent samples. TEM reveals that the heavily deformed wire consists of nanoscale fine elongated structures along the drawing direction. The diffraction patterns indicate that a substantial amount of austenite has transformed into martensite. The TEM dark field images show nanosized patches of martensite distributed among the debris of austenite along the drawing direction. The evidence strongly suggests that severe deformation leads to mechanical stabilization of austenite against the growth of martensite.

1. Introduction

In the work conducted at Kobe Steel, a remarkably high strength (about 5 GPa) has been achieved by fabricating a two-phase ferrite and martensite steel in the form of a very thin wire with a diameter of about 15–100 μm (with the trade name Scifer) [1]. The strength of Scifer is achieved by cold drawing, and the equivalent true strain is about 9. Field ion microscopy (FIM) has been utilized to reveal the atomic resolution structure [2–4]. It indicates that the deformation induces the ultra-fine dislocation cell structure with the cell size in a direction normal to the drawing direction being approximately 10–15 nm. Besides the effects of mechanical homogenization on the microstructures (due to the forced mixing of ferrite and martensite), the nanoscale dislocation substructure is believed to be the major contribution to the total strength of the wire [1, 2, 5].

The present work is an alternative study in which very strong wire has been made by cold drawing a 190 μm diameter wire of 316L austenitic stainless steel without any

*Corresponding author. Email: f89542059@ntu.edu.tw
†Present address: China Steel Co. Ltd, Kaohsiung, Taiwan, ROC.

Philosophical Magazine
ISSN 1478–6435 print/ISSN 1478–6443 online
http://www.tandf.co.uk/journals
DOI: 10.1080/14786430500254271

intermediate heat treatment to produce an 8 μm diameter wire. It has been presumed that much of the strength arises from the dislocation substructure, but the situation now appears to be complex. Austenite partly transforms to martensite during the course of drawing. This in turn is thought to lead to additional strengthening.

A better understanding of the microstructural evolution is needed to explain the strengthening mechanisms. Although the atomic resolution technique of FIM is an ideal tool for this purpose, the distribution of strain-induced martensite is not easy to identify in the image. On the other hand, it is naturally very difficult to produce samples for transmission electron microscopy from the 8 μm diameter wire. A specimen preparation method for the cross-sectional transmission electron microscopy (TEM) of the fine wire has been developed. This method is based on the typical method for TEM specimens of the edge-on cross-sectional semiconductor thin films [6–13]. Several representative TEM micrographs of the fine wire in this work will be presented and discussed.

2. Experimental procedure

AISI 316L stainless steel wires with 190 μm diameter in the fully annealed state were used as the starting material. The chemical composition of the steel is Fe–0.01C–0.75Si–17.1Cr–11.97Ni–0.53Mn–1.99Mo–0.006P–0.001S–0.046N (wt.%). Purity control is vital and the inclusion content must be kept to a minimum, since the final fibre diameter is expected to reach several microns. Beginning with 190 μm diameter wires, ultra-thin wires just 8 μm in diameter were made. There was no intermediate heat treatment used in the process of drawing, and the total amount of the true strain was about 6.3. Owing to the high amount of deformation, austenite partly induced martensitic transformation during the course of drawing, and the ultra-thin wires became magnetic.

The preparation process of the cross-sectional TEM specimen is illustrated in figure 1. One or several fine wires are stretched and then mounted between silicon chips with an epoxy adhesive (EpoxyBond 110, made by Allied High Tech Products, Inc.). The sandwiched assembly is cured at 150°C for 15 min, and then cooled down to room temperature. The bonded assembly is stuck onto a glass plate with wax (Crystal Bond 590, made by Aremco), heated to 150°C, and then cooled to the ambient temperature. The specimen–glass set is thinned initially by abrasion on silicon carbide papers with 800 and 4000-grit (as shown in figures 1b and 1c) to thin the both sides of the wafers. Attention must be paid to keeping the fine wire always parallel to the glass plate (as shown in figure 1d). McCaffrey and Hulse [14] showed that the silicon-transmitted colour changes from deep red to red in the silicon thickness range 5–10 μm; the thickness of the thinned wafer can therefore be estimated. After the wire emerges from the thinned wafer, polishing should be performed in series on diamond film wheels with particles sizes of 1, 0.5, and 0.1 μm. The final polishing is carried out on a 0.06 μm silica wheel.

Interference fringes are observable when the sample is thinner than approximately 2 μm (in this condition the silicon transmission colour appears yellow). The observation of fringes can be used as an indicator of final thickness as the foils approach perforation. Finally, the foil is mounted onto a standard copper

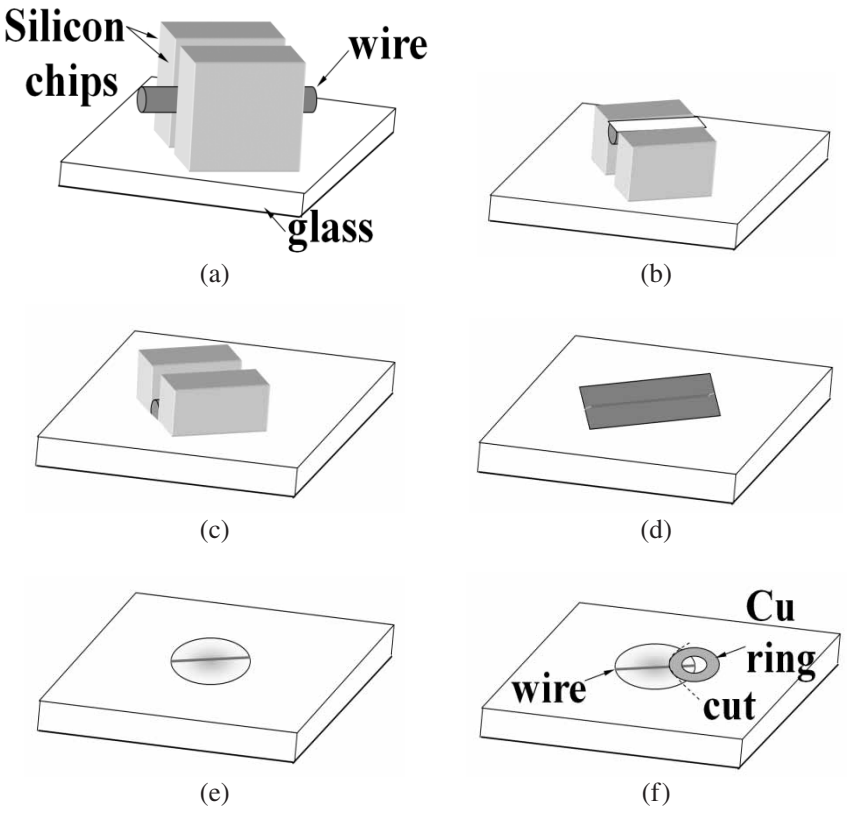

Figure 1. Schematic drawings of the cross-sectional TEM specimen preparation for the ultra-fine wires.

grid and moved into plasma cleaner for drying and cleaning before TEM observation. Ion milling is not used during the course of sample preparation in order to avoid damage caused by ion bombardment. The foils have been examined using JEM 100CX and 2000EX transmission electron microscopes operating at 100 and 200 kV, respectively.

Quantitative volume fractions of martensite and austenite have been determined by using a Brucker (AXS Type B8 Advance) X-ray diffractometer with the X-ray source of Cu-Kα ($\lambda = 1.541$ Å) operating at 30 kV and 20 mA.

3. Results and discussion

The initial structure of the 190 μm diameter wire of 316L stainless steel is presented in figure 2; it illustrates the equiaxed austenite grains with about 2 μm grain size in the fully annealed state (the annealing twins can be seen clearly). Figure 3a and b show the form of the 8 μm diameter ultra-fine wire viewed via the optical macrograph and scanning electron micrograph, respectively. Figure 4 displays

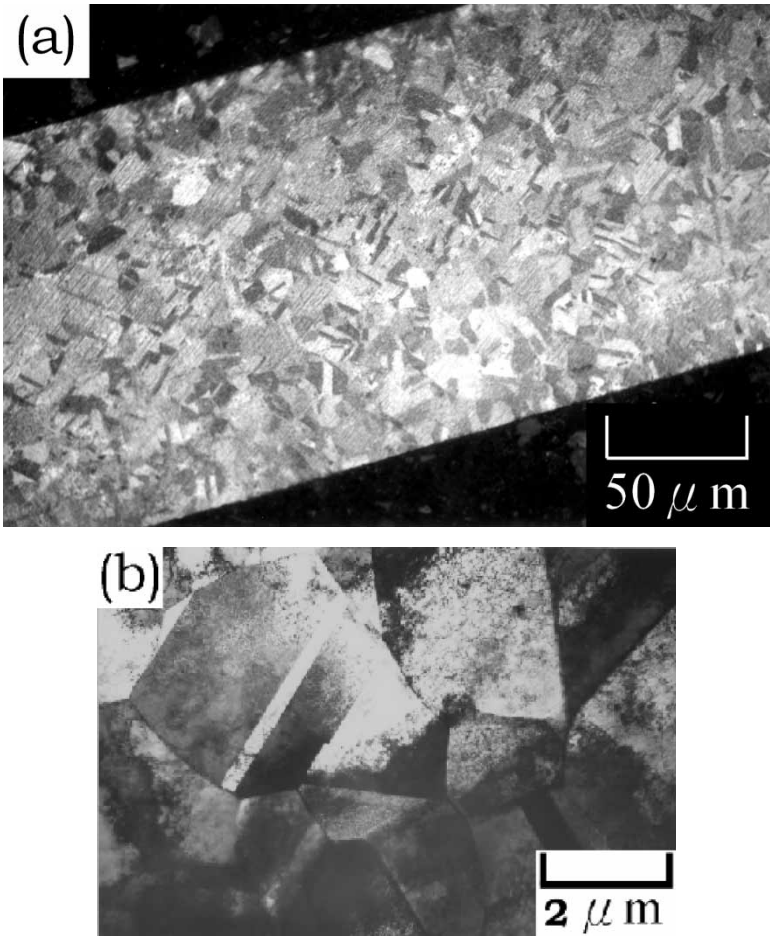

Figure 2. (a) Optical micrograph taken from the longitudinal section of the 190 μm diameter wire and (b) corresponding TEM bright field image.

low-magnification TEM micrographs taken from the transverse and longitudinal sections of the ultra-fine wire. The selected area (with an aperture diameter of 5 μm) diffraction patterns taken from the longitudinal section of the ultra-fine wire are shown in figure 5a. The corresponding analysis (figure 5b) indicates that a large amount of austenite has transformed into martensite.

Quantitative X-ray analysis has been used to determine the volume fractions of martensite and austenite in the 8 μm diameter ultra-fine wire and the 190 μm diameter wire; the X-ray diffraction spectra are shown in figure 6. In order to avoid biasing the result (figure 6b) due to the crystallographic texture in the wire, the austenite and martensite contents are calculated from the integrated intensities of (111), (200) and (220) austenite peaks, and of (110), (200), and (211) martensite peaks. It can be clearly seen that the structures before and after drawing are single phase of austenite and dual phases of austenite–martensite, separately.

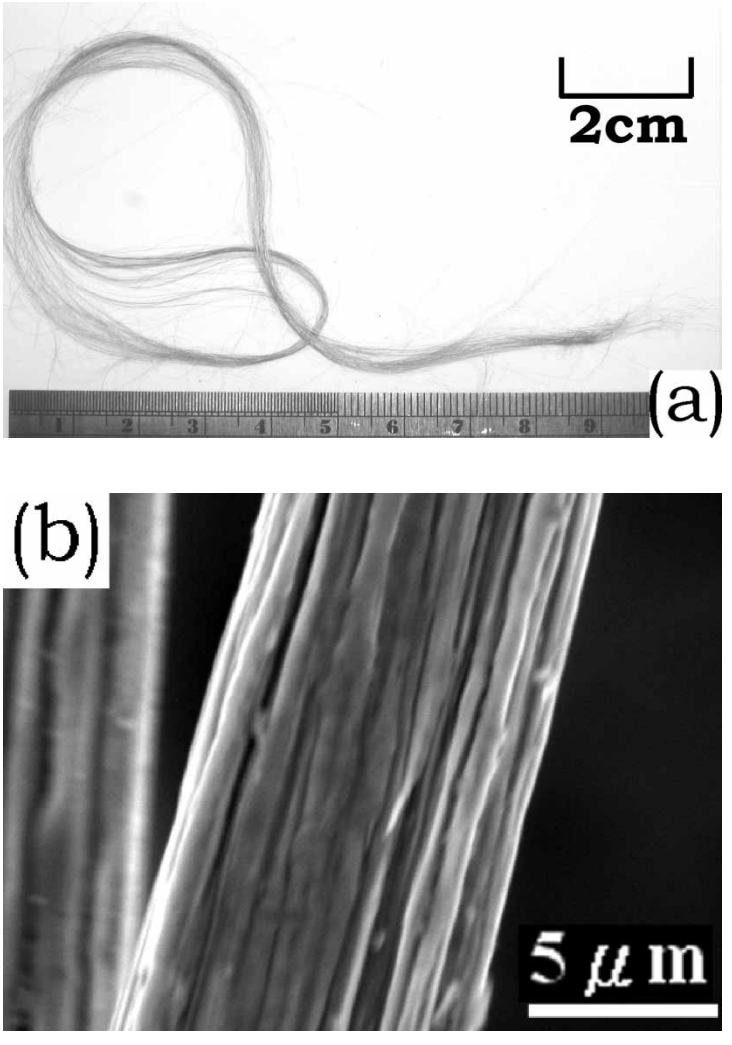

Figure 3. (a) The fibre in its final state and (b) SEM image of its surface morphology.

In the ultra-fine wire, the measured volume fractions of austenite and martensite are 0.43 and 0.57, respectively. The significance of the volume fraction of strain induced martensite will be discussed later.

Figure 7 shows TEM bright field images obtained from the transverse and longitudinal sections of the ultra-fine wire. The martensite and austenite cannot be distinguished clearly, since the heavily deformed austenite phase with extremely high strain fields exhibits a complex image contrast, similar to that produced by the strain-induced martensite phase. As a consequence of the severe cold-drawing, the nanoscale banded texture of finely elongated nanograins is observed on the longitudinal section, while the more isotropic morphology of nanograins is displayed on the transverse section. The corresponding selected area (with an aperture of 500 nm)

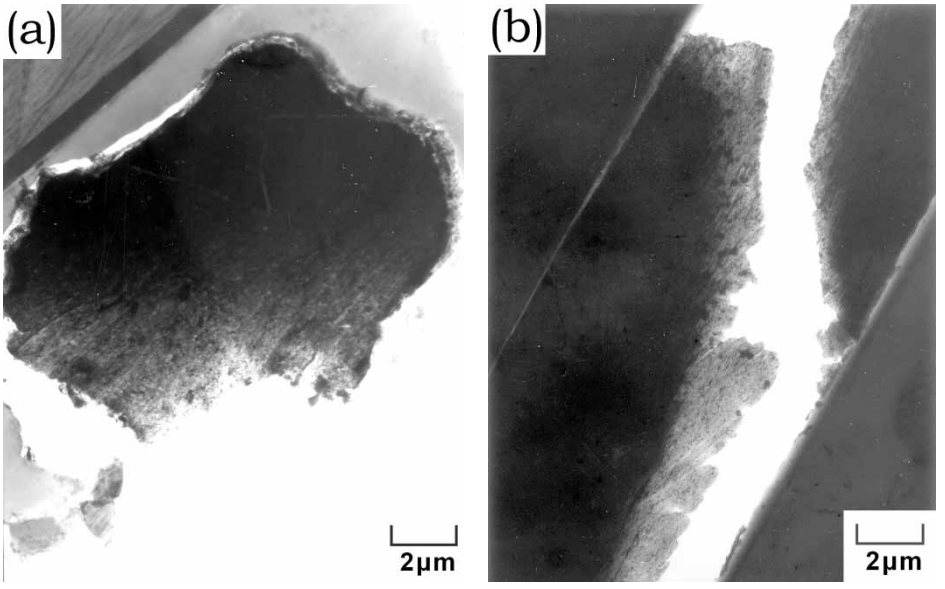

Figure 4. Low-magnification TEM taken from (a) transverse section and (b) longitudinal section of 8 μm diameter fine wire.

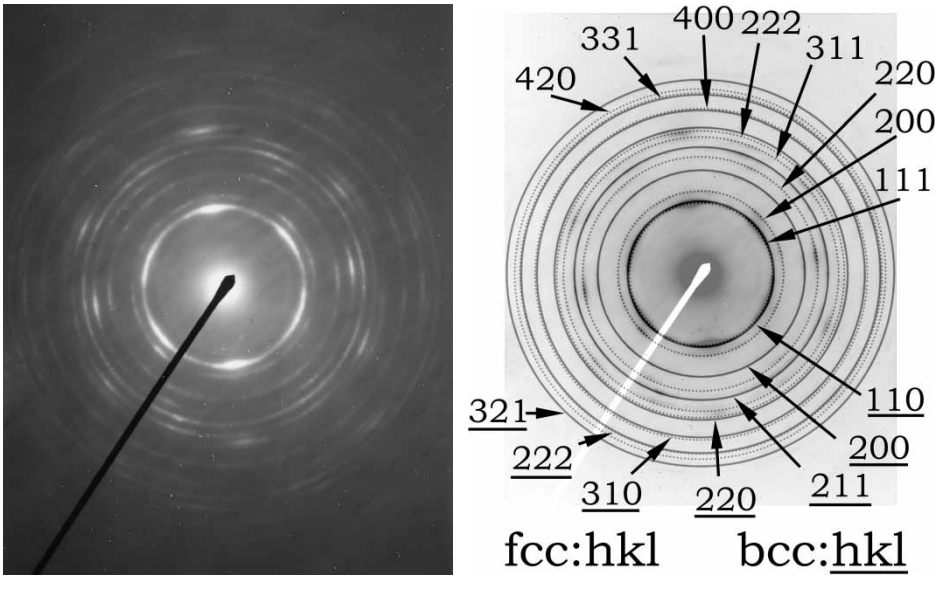

(a) (b)

Figure 5. (a) Ring-patterns obtained from the longitudinal section of the fine wire by a selected area (SA) aperture of 2 μm diameter and (b) interpretations of (a).

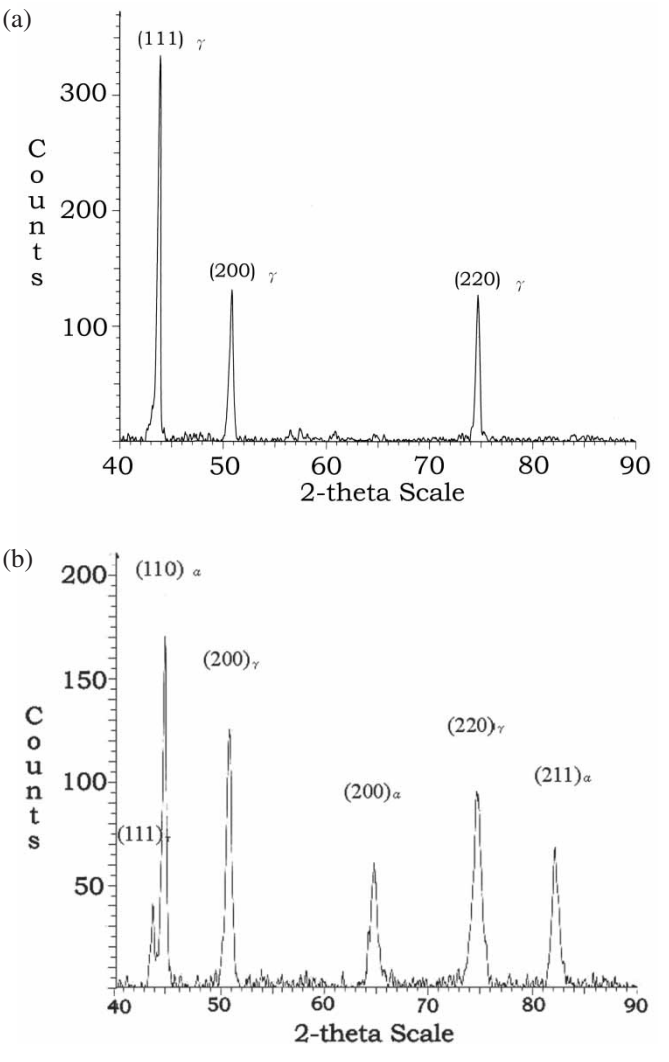

Figure 6. The X-ray diffraction spectra: (a) for the original wire with a diameter of 190 μm and (b) for the ultra-fine wire with a diameter of 8 μm.

diffraction patterns, as shown in figure 8, indicate that the preferred orientation is along the longitudinal section.

For the purpose of identifying the martensite and austenite, and investigating their sizes and distributions in the ultra-fine wire, montages of TEM dark field images taken from the longitudinal section have been completed for martensite and austenite, respectively. They are illustrated in figures 9 and 10. Because the diffraction spots from $\{110\}_{\alpha'}$ and $\{111\}_{\gamma}$ are difficult to distinguish, the dark field images of austenite and martensite are illuminated using $\{200\}_{\alpha'}$ and $\{200\}_{\gamma}$ reflections as pointed by arrows in figure 9b and c, respectively. Figure 9b illustrates that the extremely fine elongated austenite has become a row of debris; the irregularly

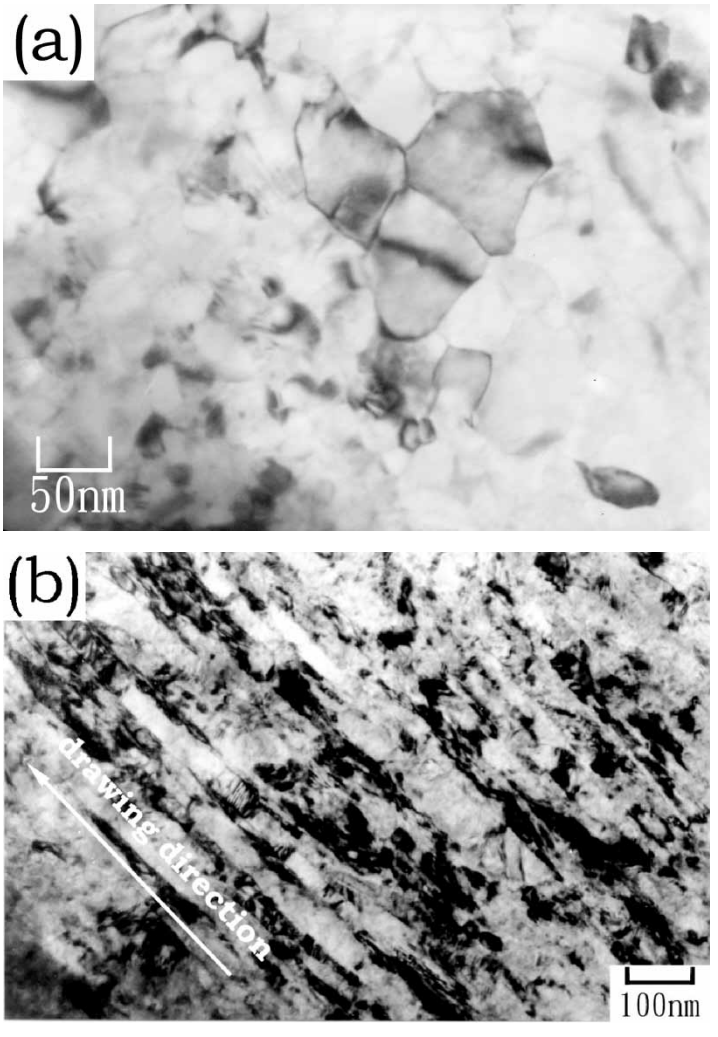

Figure 7. TEM bright field images obtained from (a) transverse and (b) longitudinal sections of the ultra-fine wire.

deformed structure of austenite presumably consists of dislocation cell structures which are slightly elongated along the drawing direction.

The state of the deformed austenite prior to transformation is of deciding importance as it influenced the nucleation sites for the strain-induced martensite. The potential nucleation sites for the embryos of martensite have been suggested to be the shear band (faults and twins) intersections [15–19]. Figure 9c shows that the newly formed martensite patches are distributed along the drawing direction. It is evident that the growth of martensite is limited. Plastic deformation is generally presumed to induce martensite nucleation, but severe deformation may cause mechanical stabilization of the austenite. This effect results from an increase in difficulty of martensite propagation into the austenite phase due to work hardening

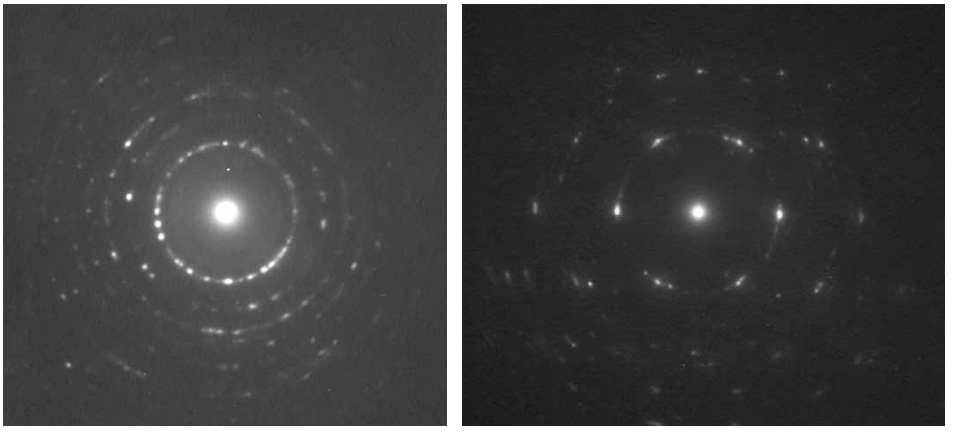

(a) (b)

Figure 8. Diffraction patterns obtained from (a) transverse and (b) longitudinal sections of the ultra-fine wire.

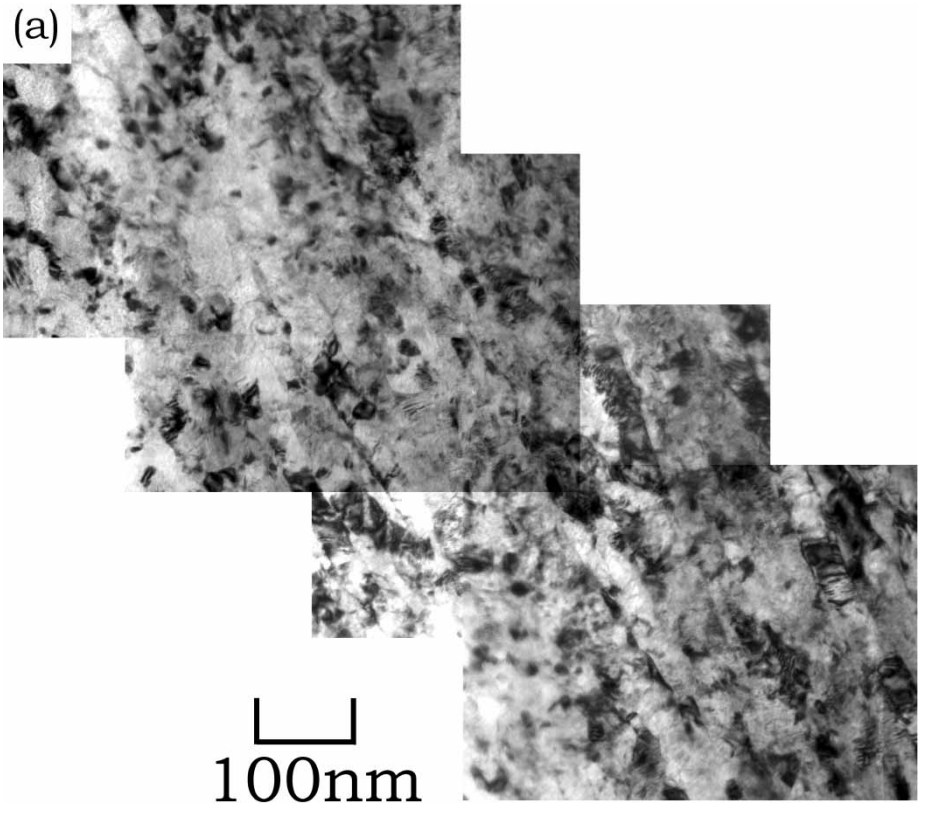

Figure 9. TEM images taken from the longitudinal section of the ultra-fine wire: (a) bright field image, (b) dark field image of austenite phase using $\{200\}_{\gamma}$ reflection and (c) dark field image of martensite phase using $\{200\}_{\alpha'}$ reflection.

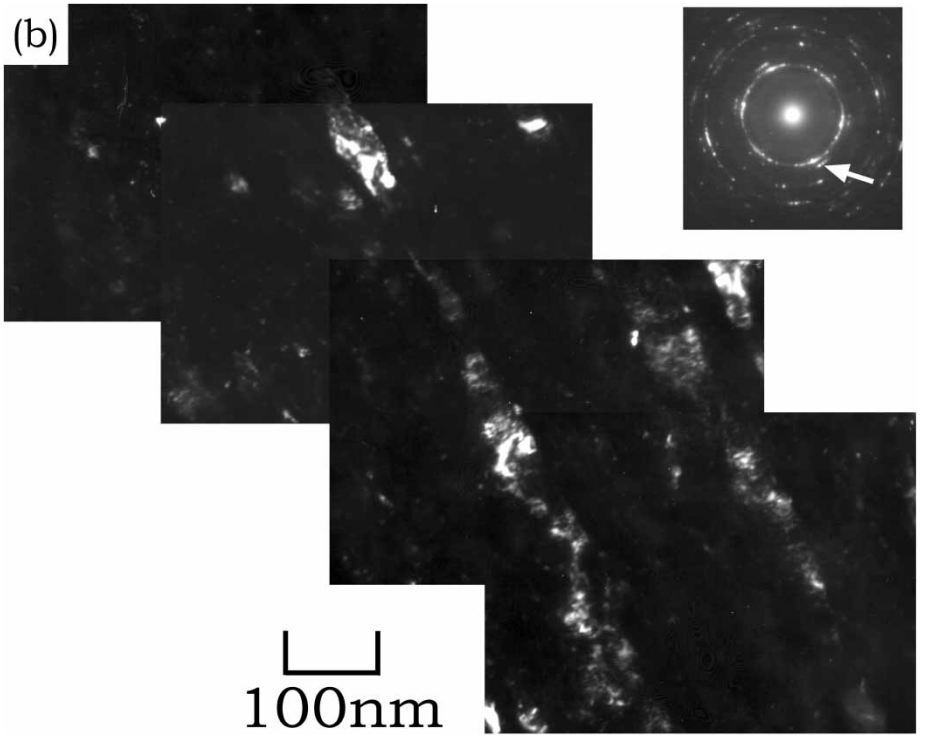

Figure 9. Continued.

of the austenite; most dislocations introduced into austenite by the cold drawing act as obstacles to interfere with the motion of glissile transformation interfaces although some of dislocations act as nucleation sites. Consequently, the heavy deformation of austenite hinders the growth of martensite. Figure 10b clearly illustrates that many patches of martensite are arrayed very closely along the drawing direction. The grains are roughly aligned and elongated along $\langle 110 \rangle_{\alpha'}$. The severe deformation leads to a high density of deformation defects and profoundly enhances the nucleation of martensite embryos.

When a single crystal of metal is plastically deformed in tension, the crystal rotates such that the slip direction approaches the tensile axis. Similarly, when the grains of polycrystalline metal are plastically deformed, all of the individual grains will rotate. However, slight deviations of the orientation occur among the all grains because each grain must undergo a deformation that allows it to conform to the changes in the shape of its neighbours. During wire drawing, the grains become elongated, and most of their crystal orientations are rotated to align with a specific crystallographic direction parallel to the wire axis, i.e. fibre texture. FCC metals often have duplex $\langle 111 \rangle$ and $\langle 100 \rangle$ fibre textures, and bcc metals have $\langle 110 \rangle$ fibre texture. In the present investigation, figure 10c–f show the selected area (with an aperture of 500 nm) diffraction patterns taken from areas A, B, C and D labelled in figure 10a. The four sets of diffraction patterns are similar and have bcc {110} or fcc {111} strong reflections. The evidence indicates that the distribution of crystal

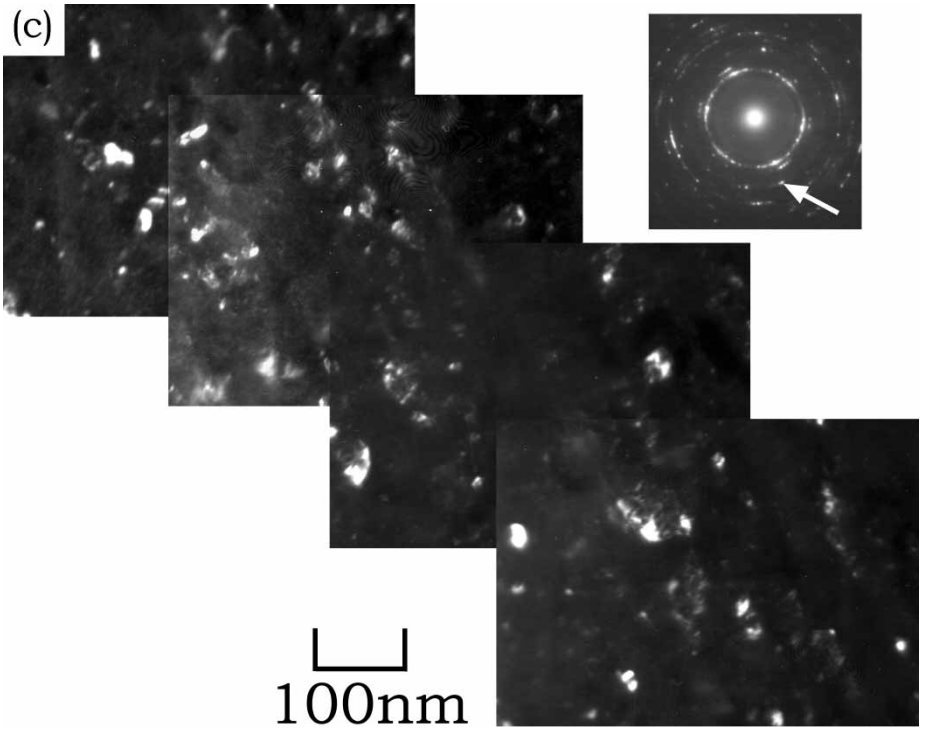

Figure 9. Continued.

orientation is non-random, although there is some scattering. However, that the diffraction patterns appear to be short arcs rather than sharp spots reflects the orientation relationships among all the grains with a given fibre texture. The detailed crystallographic relationship between the γ matrix and martensite has also been examined, as shown in figure 10g and h. It is found that the strain-induced martensite obeys Kurdjumov–Sachs (K–S) or Nishiyama–Wasserman (N–W) orientation relationships. In this work, it is strongly suggested that preferred orientations of γ matrix and newly-formed martensite exist and that the texture of martensite inherits the original deformation texture of austenite.

There is an essential difference between macroscopic yielding in large grained (micron-sized) and nanograined materials. In the former, a very large stress concentration built up due to dislocation pile-ups (on a long slip band) at a grain boundary in a given grain can generate dislocation sources in neighbouring grains. An analysis of such a process gives a Hall–Petch relationship, i.e. the macroscopic yield stress at which all grains yield depends on the inverse square root of grain size. However, for the nanograined materials, the Hall–Petch relationship is no longer applicable, because the slip band is too short. On the other hand, Langford and Cohen [20] have dealt with the problem of strengthening due to the fine dislocation cell structures formed in drawn wires. They studied the energy needed to spread dislocation loops across the glide planes of the cells, during the deformation of the dislocation cells along the wire longitudinal direction. The macroscopic yield stress was found

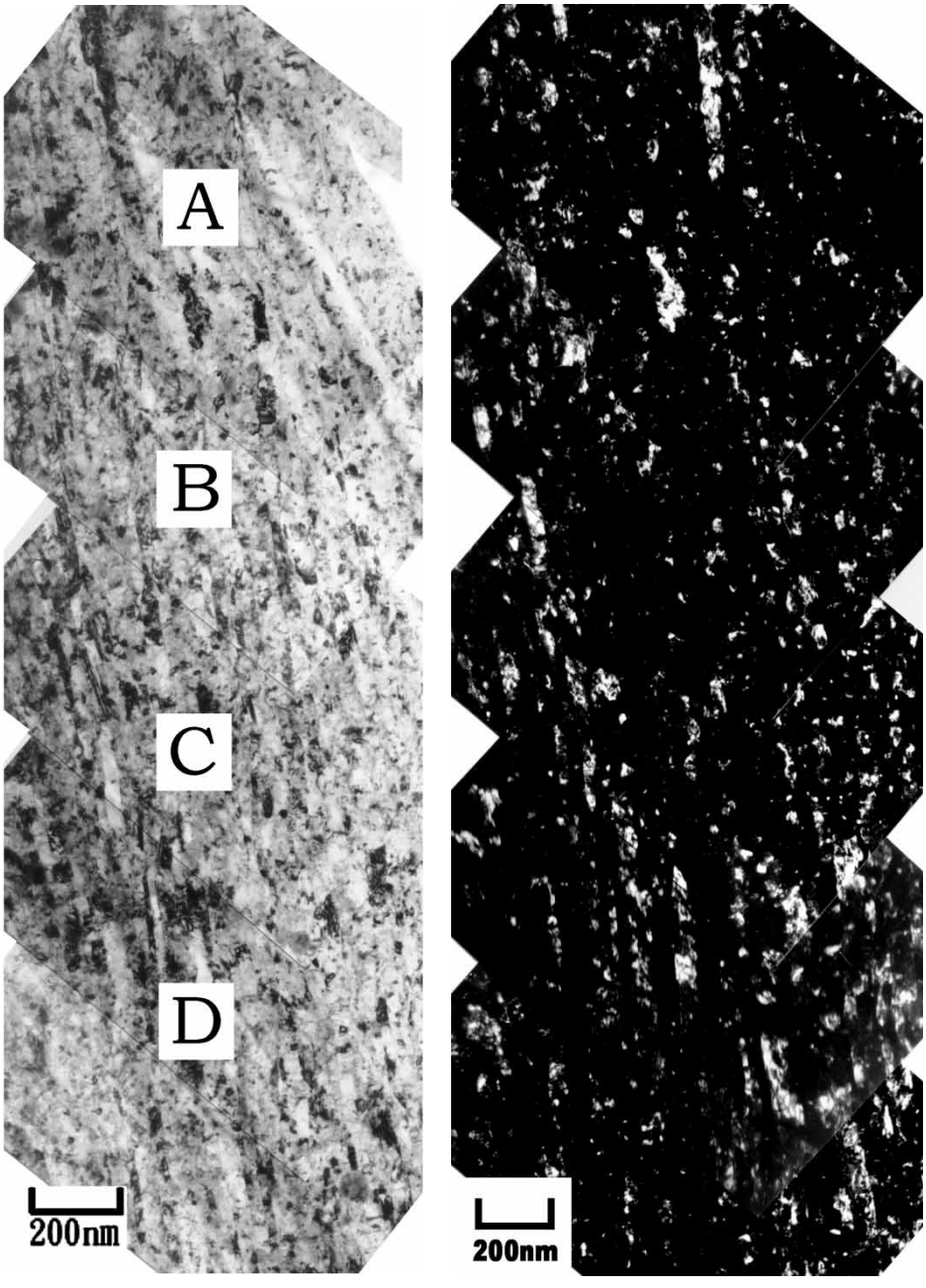

(a) (b)

Figure 10. (a) TEM bright field image taken from the longitudinal section of the fine wire and (b) the corresponding dark field image of martensite using $\vec{g} = 1\bar{1}0$, and (c)–(f) the diffraction patterns taken from areas A to D of (a), respectively; (g) and (h) represent separately the K–S and N–W orientation relationships in (f).

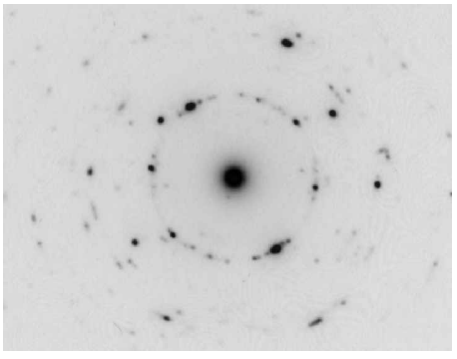

(c)

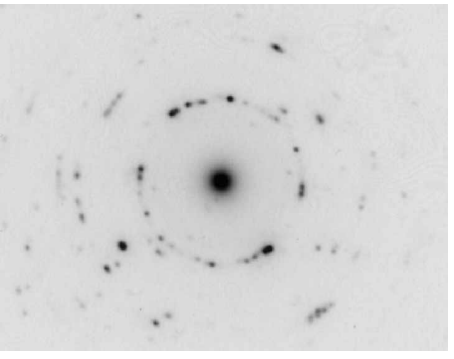

(d)

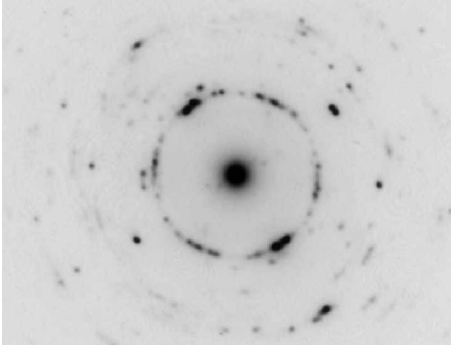

(e)

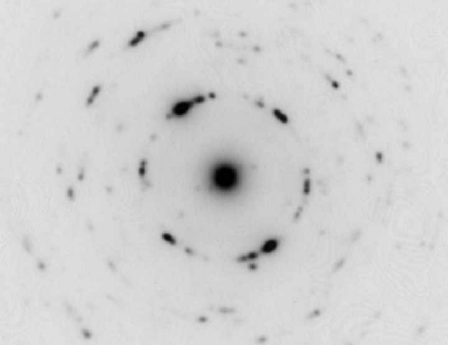

(f)

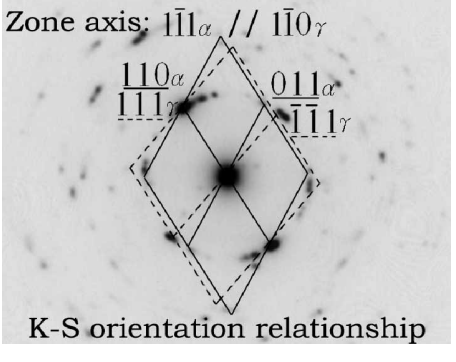

(g)

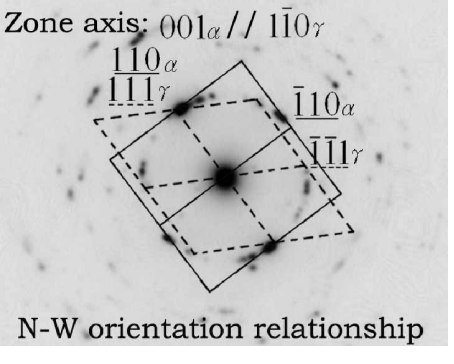

(h)

Figure 10. Continued.

to depend on the inverse of the dislocation cell size. In this work, the dislocation cell sizes of austenite and martensite in the ultra-fine wire have been estimated from the TEM dark field images as illustrated in figures 9 and 10. The cell sizes of austenite and martensite normal to the drawing direction are approximately 40–60 nm and 10–50 nm, respectively; the latter is smaller than the former, and presumed to

be the major contribution to the total strength of the wire. The yield strength of the ultra-fine wire has been measured to be about 1.24–1.59 GPa, which compares rather well with the estimated data, using the Langford–Cohen equation [20] for the yield strength of the cell structure.

Because of the attractive combination of mechanical properties and corrosion resistance, ultra-fine wires of 316L stainless steel have been increasingly used for mechanical, filtering, shielding and buffer applications in industry. For example, wire strands and ropes are particularly useful for suspension and tensioning systems; woven wire clothes are popularly used as filtration, electromagnetic wave radiation shielding, and heat-resistant buffer materials, etc. In this work, it has been shown that most of the strength of ultra-fine wires of 316L stainless steel results from the nanostructures of martensite–austenite, which are developed during cold drawing. Of more essential investigation, however, are the ageing and tempering behaviours of the extremely fine wires studied. Further research work is needed to elucidate the stability of nanostructures at elevated temperatures and to evaluate the effect of the subsequent evolution of structures on the properties.

4. Conclusions

A heavily deformed ultra-thin wire with a diameter of 8 μm has been made and characterized. A specimen preparation method for the cross-sectional TEM of ultra-fine wires has been developed. The TEM images reveal that the extremely fine elongated austenite grains have become rows of debris; the irregularly deformed structure of austenite presumably consists of nanosized dislocation cell structures. The TEM images also show that nanosized patches of newly formed martensite are distributed among the debris of austenite. It is suggested that the effect of mechanical stabilization of austenite against martensite growth leads to a large amount of nanometre-scale martensite in the ultra-fine wire. The strain-induced martensite phase has a smaller size of dislocation cell than the heavily deformed austenite phase and makes a much greater contribution to the total strength of the ultra-fine wire.

Acknowledgements

This work was carried out with the financial support from the National Science Council of Republic of China, Taiwan, under Contract NSC 92-2911-I-002-020.

References

[1] J.A. Charles, G.W. Greenwood and G.C. Smith (Editors), in *Future Developments of Metals and Ceramics* (Institute of Materials, London, 1992), pp. 25–44.
[2] H.K.D.H. Bhadeshia and H. Harada, Appl. Surf. Sci. **67** 328 (1993).
[3] H.G. Read, Scripta Mater. **37** 1221 (1997).
[4] N. Maruyama, T. Tarui and H. Tashiro, Scripta Mater. **46** 599 (2002).
[5] A.A Nazarov, Phil. Mag. A **69** 327 (1994).
[6] J.C. Braveman and R. Sinclair, J. Elec. Microsc. Tech. **1** 53 (1984).
[7] H.J. Klaar and F.Y. Hsu, Mater. Char. **36** 365 (1996).

[8] R.S. Hay, J.R. Welch and M.K. Cinibulk, Thin Solid Films **308–309** 389 (1997).
[9] E. Muller and F. Krumeich, Ultramicrosc. **84** 143 (2000).
[10] J.Y. Dai, S.F. Tee, C.L. Tay, Z.G. Song, S. Ansari, E. Er and S. Redkar, Microelec. J. **32** 221 (2001).
[11] J.B. Park, Y.S. Cho, S.Y. Hong, *et al*. Thin Solid Films **415** 78 (2002).
[12] D. Eyidi and O. Eibl, Micron **33** 499 (2002).
[13] A. Montone and M. Vittori Antisari, Micron **34** 79 (2003).
[14] J.P. McCaffrey and J. Hulse, Micron **29** 139 (1998).
[15] T. Inamura, K. Takashima and Y. Higo, Phil. Mag. **83** 935 (2003).
[16] L.E. Murr, K.P. Staudhammer and S.S. Hecker, Metall. Trans. A **13** 627 (1982).
[17] V. Shrinivas, S.K. Varma and L.E. Murr, Metall. Mater. Trans. A **26** 661 (1995).
[18] P.L. Mangonon Jr. and G. Thomas, Metall. Trans. **1** 1577 (1970).
[19] D.C. Cook, Metall. Trans. A **18** 201 (1987).
[20] G. Langford and M. Cohen, Metall. Trans. **1** 1478 (1970).